J|A|C|S
A R T I C L E S

Origin of Photoactivity of Nitrogen-Doped Titanium Dioxide under Visible Light

Stefano Livraghi,[†] Maria Cristina Paganini,[†] Elio Giamello,*,[†] Annabella Selloni,[‡] Cristiana Di Valentin,[§] and Gianfranco Pacchioni[§]

Contribution from the Dipartimento di Chimica IFM, Università di Torino and NIS Center of Excellence, Via P. Giuria 7, 10125 Torino, Italy, Department of Chemistry, Princeton University, Princeton, New Jersey 08540, Dipartimento di Scienza dei Materiali, Università di Milano-Bicocca, Via R. Cozzi, 53, 20125 Milano, Italy

Received June 13, 2006; E-mail: elio.giamello@unito.it

Abstract: Nitrogen-doped titanium dioxide (N-TiO$_2$), a photocatalytic material active in visible light, has been investigated by a combined experimental and theoretical approach. The material contains single-atom nitrogen impurities that form either diamagnetic (N$_b^-$) or paramagnetic (N$_b^•$) bulk centers. Both types of N$_b$ centers give rise to localized states in the band gap of the oxide. The relative abundance of these species depends on the oxidation state of the solid, as, upon reduction, electron transfer from Ti^{3+} ions to N$_b^•$ results in the formation of Ti^{4+} and N$_b^-$. EPR spectra measured under irradiation show that N$_b$ centers are responsible for visible light absorption with promotion of electrons from the band gap localized states to the conduction band or to surface-adsorbed electron scavengers. These results provide a characterization of the electronic states associated with N impurities in TiO$_2$ and, for the first time, a picture of the processes occurring in the solid under irradiation with visible light.

1. Introduction

An intense research activity has been recently devoted to the preparation and characterization of titanium dioxide (TiO$_2$) materials doped with nonmetal impurities. The goal is to produce an active photocatalyst which can work under visible light, rather than UV irradiation, so that sunlight can be more efficiently used in photocatalysis. One of the most promising and widely investigated systems in this respect is nitrogen-doped titanium dioxide, N-TiO$_2$, which shows a significant catalytic activity in various reactions performed under visible light irradiation.[1−13] The potential technological impact of this system is huge, and

some practical applications have already appeared on the market. Recently, also a highly efficient dye-sensitized solar cell (DSC) was fabricated using a nanocrystalline nitrogen-doped titania electrode.[14]

To incorporate nitrogen in titanium dioxide, different strategies are used, either based on chemical reactivity (sol−gel synthesis,[1,3,7−9] chemical treatments of the bare oxide,[2,4,5,12] oxidation of titanium nitride,[15] etc.) or on physical methods (ion implantation,[16−18] magnetron sputtering[19,20]). These different procedures probably lead, at least in some cases, to materials with somewhat different properties. Independent of the preparation method, one of the key points under debate concerns the chemical nature and the location in the solid of the species responsible for the photoactivity in visible light. Different chemical species like NO$_x$[1,3,9,21−23] substitutional N,[2,6,8,16] or NH$_x$[5] have been proposed as responsible of this effect. Several nitrogen-containing species are actually produced during the

[†] Università di Torino and NIS Center of Excellence.
[‡] Princeton University.
[§] Università di Milano-Bicocca.
(1) Sato, S. *Chem. Phys. Lett.* **1986**, *123*, 126−128.
(2) Asahi, R.; Morikawa, T.; Ohwaki, T.; Aoki, K.; Taga, Y. *Science* **2001**, *293*, 269−271.
(3) Sakthivel, S.; Janczarek, M.; Kisch, H. *J. Phys. Chem. B* **2004**, *108*, 19384−19387.
(4) Irie, H.; Watanabe, Y.; Hashimoto, K. *J. Phys. Chem. B* **2003**, *107*, 5483−5486.
(5) Diwald, O.; Thompson, T. L.; Zubkov, T.; Goralski, E. G.; Walck, S. D.; Yates, J. T., Jr. *J. Phys. Chem. B* **2004**, *108*, 6004−6008.
(6) Miyauchi, M.; Ikezawa, A.; Tobimatsu, H.; Irie, H.; Hashimoto, K. *Phys. Chem. Chem. Phys.* **2004**, *6*, 865−870.
(7) Gole, J. L.; Stout, J. D.; Burda, C.; Lou, Y.; Chen, X. *J. Phys. Chem. B* **2004**, *108*, 1230−1240.
(8) Lin, Z.; Orlov, A.; Lambert, R. M.; Payne, M. C. *J. Phys. Chem. B* **2005**, *109*, 20948−20952.
(9) Sato, S.; Nakamura, R.; Abe, S. *Appl. Catal., B* **2005**, *284*, 131−137.
(10) Sathish, M.; Viswanathan, B.; Viswanath, R. P.; Gopinath, C. S. *Chem. Mater.* **2005**, *17*, 6349−6353.
(11) Alvaro, M.; Carbonell, E.; Fornés, V.; Garcia, H. *ChemPhysChem* **2006**, *7*, 200−205.
(12) Nosaka, Y.; Matsushita, M., Nasino, J.; Nosaka, A. Y. *Sci. Technol. Adv. Mater.* **2005**, *6*, 143−148.
(13) Irokawa, Y.; Morikawa, T.; Aoki, K.; Kosaka, S.; Ohwaki, T.; Taga, Y. *Phys. Chem. Chem. Phys.* **2006**, *8*, 1116−1121.

(14) Ma, T. L.; Akiyama, M.; Abe, E.; Imai, I. *Nano Lett.* **2005**, *5*, 2543−2547.
(15) Morikawa, T.; Asahi, R.; Ohwaki, T.; Aoki, K.; Taga, Y. *Jpn. J. Appl. Phys.* **2001**, *40*, L561−L563.
(16) Diwald, O.; Thompson, T. L.; Goralski, E. G.; Walck, S. D.; Yates, J. T., Jr. *J. Phys. Chem. B* **2004**, *108*, 52−57.
(17) Batzill, M.; Morales, E. H.; Diebold, U. *Phys. Rev. Lett.* **2006**, *96*, 026103.
(18) Ghicov, A.; Macak, J. M.; Tsuchiya, H.; Kunze, J.; Haeublein, V.; Frey, L.; Schmuki, P. *Nano Lett.* **2006**, *6*, 1080−1082.
(19) Mwabora, J. M.; Lindgren, T.; Avendano, E.; Jaramillo, T. F.; Lu, J.; Lindquist, S. E.; Granqvist, C. G. *J. Phys. Chem. B* **2004**, *108*, 20193−20198.
(20) Nakano, Y.; Morikawa, T.; Ohwaki, T. Taga, Y. *Appl. Phys. Lett.* **2005**, *86*, 132104.
(21) Chen, X.; Burda, C. *J. Phys. Chem. B* **2004**, *108*, 15446−15449.
(22) Sakatani, Y.; Nunoshige, J.; Ando, H.; Okusako, K.; Koike, H.; Takata, T.; Kondo, J. N.; Hara, M.; Domen, K. *Chem. Lett.* **2003**, *32*, 1156−1157.
(23) Di Valentin, C.; Pacchioni, G.; Selloni, A.; Livraghi, S.; Giamello E. *J. Phys Chem. B* **2005**, *109*, 11414−11419.

chemical treatments leading to the final N-TiO$_2$ material, and the main problem is to identify the species present in the system and to rationalize the role of each of them. In other words, one needs to distinguish between inert byproducts of the chemical preparation, unavoidably present in the solid, and species which are playing an effective role in visible light absorption and molecular (photo) activation. This is also useful for choosing the most convenient preparation method for the photocatalyst.

A second key issue concerns the electronic structure of the doped material and its modification upon irradiation. This question has been addressed in a number of computational studies, but no general consensus has been reached yet. While some authors claim that the band gap of the solid is reduced due to a rigid valence band shift upon doping[2,15,20] (the gap is 3.2 eV, corresponding to UV radiation, for undoped anatase TiO$_2$), others attribute the observed absorption of visible light by N-TiO$_2$ to the excitation of electrons from localized impurity states in the band gap.[3,4,6,9,10]

A significant advance toward a clarification of the above issues has been recently achieved by means of electron paramagnetic resonance (EPR) spectroscopy measurements and DFT calculations. Due to the sensitivity and capability of EPR to directly describe the electronic structure of a paramagnetic center, this technique has assumed, in the past 40 years, a paramount importance in the investigation of point defects in insulators and semiconductors.[24] In the case of N-TiO$_2$ prepared via sol–gel synthesis, EPR has evidenced, inter alia, the existence of a paramagnetic nitrogen species intimately interacting with the TiO$_2$ lattice. The spin-Hamiltonian parameters of such a species are consistent with calculations for both substitutional and interstitial N impurities.[23] In the substitutional case, corresponding to a nitrogen atom replacing an oxygen at a regular lattice site, calculations show that the impurity energy levels are just above the top of the valence band,[25] whereas in the case where the N atom is hosted in an interstitial position, directly bound to a lattice oxygen, the impurity states are found to lie slightly higher in the gap.[23] Although not proven experimentally, it was inferred from theory that excitations from these localized states could explain the visible light absorption of the yellow N-TiO$_2$ material and the consequent activity in visible light. However, conclusive evidence for this picture has not yet been found.

In this paper we describe a series of experiments aimed at investigating the behavior of sol–gel prepared N-TiO$_2$ under irradiation with photons of different energy and in the presence of adsorbates. We unambiguously show that the above-mentioned N-species is indeed connected to the absorption of visible radiation and to the photoinduced electron transfer from the solid to a surface-adsorbed electron scavenger as molecular oxygen. By coupling these experiments with state-of-the-art DFT calculations we provide, for the first time, a consistent detailed picture of the electronic states associated with the N impurity and a mechanistic picture of the processes occurring in the solid during visible light irradiation and photoactivation of adsorbed molecules.

2. Experimental Section

2.1. Synthesis and basic characterization of the materials. Bare TiO$_2$ and N-TiO$_2$ were prepared via sol–gel, mixing a solution of titanium (IV) isopropoxide in isopropyl alcohol with water, in the former case, and with an NH$_4$Cl solution in the case of N-TiO$_2$. All reactants

employed in this work were purchased by Aldrich and used without any other purification treatment. The mixture was kept under stirring at room temperature until a complete hydrolysis was reached. The gels prepared in this way were left aging for 15 h at room temperature, subsequently dried at 340 K for 4 h and eventually calcined in air at 770 K. Both samples have a surface area of about 90 m^2 g^{-1} which was measured by the BET method and anatase structure as measured by X-ray diffraction. The N-doped titanium dioxide exhibits a pale-yellow color. Prior to the spectroscopic analysis and in order to remove the physisorbed water, the material was outgassed at room temperature until a residual pressure of about 10^{-6} kPa was reached.

2.2. Experimental Methods. Structural features of the prepared materials have been determined by X-ray Diffraction (XRD) on a Philips 1830 XRD spectrometer using a Kα Co source. UV–vis diffuse reflectance (DR UV–vis) spectra were recorded by a Varian Cary 5/UV–vis–NIR spectrometer using a Cary win-UV scan software to follow the visible absorption enhancement after nitrogen doping. Electron paramagnetic resonance (EPR) spectra were run using a X-band CW-EPR Bruker EMX spectrometer equipped with a cylindrical cavity operating at 100 kHz field modulation and a temperature controller unit. The measurements were carried out in cells that can be connected to a conventional high-vacuum apparatus (residual pressure <10^{-6} kPa). The EPR spectra intensity has been obtained by double integration of the signal. The evaluation of the intensity of each single component in spectra composed by two or more overlapping species has been derived by a computer simulation of the signal performed using SIM32, a program elaborated by Z. Sojka (Jagellonian University, Cracow).[26] The effect of visible light on EPR spectra was investigated directly irradiating the sample into the EPR cavity using a 500 W mercury/xenon lamp (Oriel instruments) equipped with a IR water filter and a grating monocromathor with a transmission range between 500 and 180 nm.

2.3. Computational Details. The calculations have been performed using the plane-wave-pseudopotential approach together with the Perdew–Burke–Ernzerhof (PBE) exchange correlation functional,[27] as implemented in the ν-ESPRESSO package.[28] The Car–Parrinello approach[29,30] was employed for geometry optimizations, with the Brillouin zone sampling limited to the Γ point, while the PWSCF code[28] was used to refine the calculations by including low-symmetry k-points, and to obtain electronic band structures and the energetics of the processes. An almost cubic bulk anatase $2\sqrt{2} \times 2\sqrt{2} \times 1$ supercell containing 96 atoms was used. Substitutional N-doping (N$_s$• species) was modeled by replacing one oxygen atom in this supercell, while interstitial N-doping (N$_i$• species) was modeled by adding one N atom in the supercell. In the following, the paramagnetic species will be denoted as N$_b$•, where b stands for bulk, when the distinction between N$_i$• and N$_s$• is irrelevant for the discussion. When studying oxygen vacancy formation, one oxygen atom was removed, while either two other oxygen atoms were replaced with N atoms or two N atoms were added in interstitial positions. The supercell models are overall neutral despite the fact that the isolated defects are charged (as described below) in order to reflect the experimental situation. The resulting stoichiometry is TiO$_{2-3x}$N$_{2x}$ with $x = 0.031$, so that the N concentration is comparable to that used in the experiments. Atomic relaxations were carried out using a second-order damped dynamics until all components of the residual forces were less than 0.025 eV/Å. For further computational details, see ref 23 and 25.

(24) Spaeth, J. M., Overhof, H., Eds. *Point Defects in Semiconductors and Insulators*; Springer-Verlag: New York, 2004.
(25) Di Valentin, C.; Pacchioni, G.; Selloni, A. *Phys. Rev. B: Solid State* **2004**, *700*, 85116.
(26) Adamski, A.; Spalek, T.; Sojka, Z. *Res. Chem. Indermed.* **2003**, *29*, 793–804.
(27) Perdew, J. P.; Burke, K.; Ernzerhof, M. *Phys. Rev. Lett.* **1996**, *77*, 3865–3868.
(28) Baroni, S. et al.: http://www.pwscf.org.
(29) Car, R.; Parrinello, M. *Phys. Rev. Lett.* **1985**, *55*, 2471–2474.
(30) Laasonen, K.; Pasquarello, A.; Car, R.; Lee, C.; Vanderbilt, D. *Phys. Rev. B: Solid State* **1993**, *47*, 10142–10153.
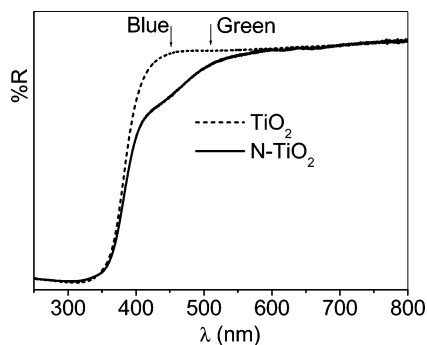
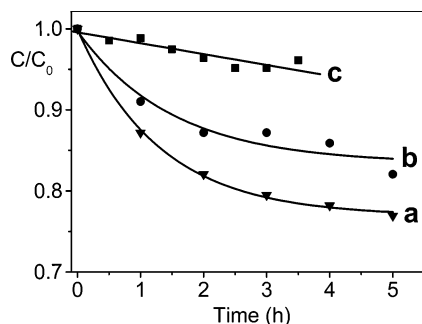**Figure 1.** UV−vis diffuse reflectance spectra of bare and N-doped TiO_2.

Figure 2. Rate of methylene blue degradation under irradiation with visible light in the presence of (a) N-doped material, (b) bare TiO_2, (c) blank. C_0 is the initial concentration of methylene blue and C, the concentration at a given time.

Standard density functionals do not properly describe band gaps and impurity levels in semiconductors, while hybrid functionals can successfully overcome these difficulties.[31,32] However, in the present context there is no need to use hybrid functionals for two reasons: 1) the position of the N-impurity states is not altered when computed with the B3LYP hybrid functional[23] which correctly describes the band gap of TiO_2; 2) when considering the concomitant presence of N-impurities and oxygen vacancies, there are no excess electrons in Ti^{3+} states (poorly described by standard DFT),[32] as they are transferred to the empty N-states (see below). Even if the original position of the Ti^{3+} states is not accurately given by PBE, there is no doubt that these states are higher in energy than those associated with the N impurities. Thus, internal charge transfer occurs independently of the exchange-correlation functional used.

3. Results and Discussion

3.1. Optical Absorption and Photocatalytic Activity of N−TiO_2. Figure 1 compares the diffuse reflectance (DR) UV−vis spectra of bare and N-doped TiO_2 prepared via sol−gel. The two spectra essentially differ for the broad absorption in the visible region centered at about 450 nm (blue) which characterizes the doped material.

The spectrum in Figure 1 is very similar to that reported by Sato,[1] who first obtained N-TiO_2 in 1986, and to the spectra reported by other authors[4,9,33,34] as well. The photocatalytic activity of the materials has been tested in the degradation reaction of methylene blue (MB; Figure 2) using monochromatic light (437 nm) and following a procedure already reported by Burda et al.[35] The reaction rate in the presence of N-TiO_2 (Figure
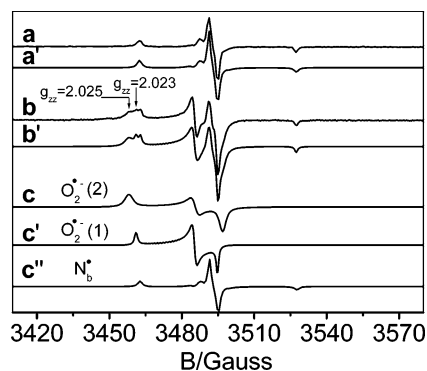
(31) Pacchioni, G., Frigoli, F.; Ricci, D.; Weil, J. A. *Phys. Rev. B*: *Solid State* **2001**, *63*, 054102.
(32) Di Valentin, C.; Pacchioni, G.; Selloni, A. *Phys. Rev. Lett.* **2006**, *97*, 166803.
(33) Yin, S.; Zhang, Q.; Sato, F.; Sato, T. *Chem. Lett.* **2003**, *32(4)*, 358−359.
(34) Kuroda, Y.; Mori, T.; Yagi, K.; Makimata, N.; Kawahara, Y.; Nagao, M.; Kittaka, S. *Langmuir* **2005**, *21*, 8026−8034.

Figure 3. EPR spectra and corresponding simulations of $N_b^\bullet$ species and surface adsorbed $O_2^{\bullet-}$. (a) $N_b^\bullet$, experimental spectrum; (a′) $N_b^\bullet$, simulation; (b) $N_b^\bullet$ and $O_2^{\bullet-}$, experimental spectrum; (b′) $N_b^\bullet$ and $O_2^{\bullet-}$, simulation; (c, c′, c″) deconvolution of signal b ($N_b^\bullet$, $O_2^{\bullet-}$ (1), $O_2^{\bullet-}$ (2), Table 1).

Table 1. Spin-Hamiltonian Parameters of the Species Identified by EPR

species	g_1	g_2	g_3	$^N A_1(G)$	$^N A_2(G)$	$^N A_3(G)$
$N_b^\bullet$	2.005	2.004	2.003	2.3	4.4	32.2

	g_{zz}	g_{yy}	g_{xx}			
$O_2^{\bullet-}$ (1)^a	2.023	2.009	2.004	/	/	/
$O_2^{\bullet-}$ (2)^a	2.025	2.009	2.003	/	/	/

^{a} The two signals are due to superoxide species stabilized on two surface Ti^{4+} ions which slightly differ in terms of coordinative environment (see text).
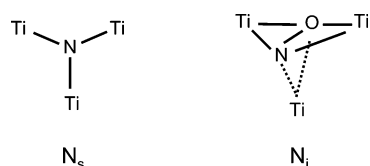
2a) was compared with that obtained using bare TiO_2 (Figure 2b). A non-negligible reduction of the MB concentration in solution is also shown by the bare TiO_2 sample which seems essentially due to surface adsorption of the reactant and photodegradation of adsorbed molecules. Noncatalytic degradation of MB in solution also occurs and its trend has been monitored by the blank test in Figure 2c. The most relevant information coming from the experiment in Figure 2 is that the activity of N-TiO_2 in photodegradation of MB is definitely (though not largely) higher than that of the bare oxide. This is in line with results previously reported in the literature.[7,35−37]

3.2. The $N_b^\bullet$ Center. EPR Spectra and Behavior upon Redox Treatments. Previous work from our laboratories[23,28] identified two distinct N-containing paramagnetic species in N-doped TiO_2. One of these species, molecular NO^{38} segregated in closed pores within the crystals, does not influence the electronic structure of the solid. The other species (Figure 3a, Table 1 first row), which is the one of interest, is characterized by a rhombic **g** tensor with the principal values extremely close one to the other and by a hyperfine structure based on a main triplet of lines ($A_3 = 32.2$ G) and two minor triplets, A_1 and A_2, centered on g_1 and g_2, respectively. This clearly indicates the presence of a single N atom in the species. The absence of H hyperfine lines in the spectrum rules out the presence of NH_x paramagnetic fragments. By recording the EPR spectrum at 77 K in the presence of a surface physisorbed O_2 multilayer, the line width of the signal reported in Figure 3a remains unchanged,

(35) Burda, C.; Lou, Y.; Chen, X.; Samia, A. C.; Stout, S.; Gole, J. J. L. *Nano Lett.* **2003**, *3*, 1049−1051.
(36) Wei, H. Y.; Wu, Y. S.; Lun, N.; Zhao, F. *J. Mater. Sci.* **2004**, *39*, 1305−1308.
(37) Sathish, M.; Viswanathan, B.; Viswanath, R. P.; Gopinath, C. S. *Chem. Mater.* **2005**, *17*, 6349−6353.
(38) Livraghi, S.; Votta, A.; Paganini, M. C.; Giamello, E. *Chem. Commun.* **2005**, 498−500.

Scheme 1

N_s N_i

Figure 4. Electronic band structure modifications resulting from the interactions between $N_b^{\bullet}$ ($N_s^{\bullet}$ or $N_i^{\bullet}$) and Ti^{3+} (oxygen vacancy) defects.

indicating that no dipolar interaction is established between the species and the paramagnetic oxygen molecules. This result allows us to exclude that the paramagnetic entity under investigation is a surface-anchored species, and rather suggests that its nature is that of a bulk diluted paramagnetic center.

The spin-Hamiltonian parameters of $N_b^{\bullet}$ (b = bulk), reported in Table 1, appear to be compatible with those calculated from first principles DFT for a N atom in interstitial position within the anatase TiO$_2$ lattice, $N_i^{\bullet}$, even though the computed hyperfine constants for a substitutional N impurity at an oxygen site, $N_s^{\bullet}$, are also quite similar[23] (Scheme 1).

Whatever the precise nature of the nitrogen centers, an important point is that, at variance with other diamagnetic and paramagnetic species observed in N-TiO$_2$, the species is stable upon washing and calcination in air up to 773 K. This indicates a deep interaction of the $N_b^{\bullet}$ center with the solid matrix. Furthermore, the intensity of the EPR signal from this center dramatically decreases when the solid is outgassed at 773 K (a treatment that is known to cause oxygen depletion, and thus reduction of TiO$_2$), and reversibly reappears after reoxidation in O$_2$ at the same temperature. This indicates that the energy levels of the N-species are part of the electronic structure of the solid and that their population is affected by the structural or electronic modifications induced by reduction of the material. The details of this interaction have been clarified by means of DFT calculations.

3.3. Electronic Structure of N-TiO$_2$: Influence of Oxygen Vacancies on N_b States. To study the interplay between N impurities and oxygen vacancies, DFT calculations have been performed for a bulk supercell of 96 atoms (anatase phase) containing either two $N_i^{\bullet}$ or two $N_s^{\bullet}$ paramagnetic species plus an oxygen vacancy located as far as possible from the N-centers, so as to avoid any direct defect−impurity interaction. It is well-established[39−41] that the excitation under irradiation in TiO$_2$ essentially produces electron−hole pairs in the bulk. These charge carriers rapidly diffuse (in the nanosecond regime) to the surface unless they are trapped or recombine. Therefore, though some surface impurities may, in principle, exist and play some role, we have focused our attention on those bulk impurities which indeed exist and interact with visible photons and we have investigated the relationship between the induced impurity states and the photoabsorption in the visible.

An oxygen vacancy in TiO$_2$ is characterized by the presence of two excess electrons which cause reduction of two Ti^{4+} cations and formation of Ti^{3+} ions. The states of the latter are experimentally found to be about 0.8 eV below the bottom of the conduction band.[42,43] The electrons are localized in the 3d orbitals of the Ti^{3+} ions, thus resulting in a magnetic resonance detected by EPR experiments.[44−46]
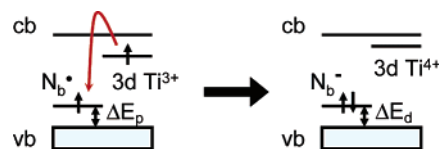
Due to the presence of two $N_b^{\bullet}$ centers and one oxygen vacancy per supercell, various spin configurations need to be considered in the calculations. In particular, the high-spin configuration corresponds to four unpaired electrons (quintet state), two on the two N-impurities and two on two Ti^{3+} ions, while a low-spin closed shell configuration (singlet state) results from the charge transfer of the two unpaired electrons occupying the high-lying Ti^{3+} states to the low-lying $N_i^{\bullet}$ and/or $N_s^{\bullet}$ singly occupied levels, just above the top of the valence band (Figure 4). This process leads to the formation of charged diamagnetic N_i^{-} and N_s^{-} defects and reoxidized Ti^{4+} ions. The low-spin configuration is found to be about 3 eV *more stable* than the high-spin quintet one. Another possible internal charge-transfer causing spin pairing directly involves the $N_i^{\bullet}$ and $N_s^{\bullet}$ centers, with formation of N_i^{+} and N_s^{-}. However, the associated energy gain is tiny, 0.1 eV, and this second charge transfer is probably not playing a direct role in the process under investigation. In all cases, the formation of charged defects in the material is accompanied by a local distortion: the N_s^{-} center is characterized by shorter N−Ti bond lengths than $N_s^{\bullet}$; N_i^{-} by a longer NO bond length than $N_i^{\bullet}$.

Similar to their neutral counterparts, the diamagnetic N_i^{-} and N_s^{-} charged defects give rise to localized levels in the gap of the material which lie a few tenths of an eV above the valence band edge. Because of the increased Coulombic repulsion, the N-induced defect states for the diamagnetic charged species are slightly higher in energy than the corresponding singly occupied levels for the paramagnetic neutral species: 0.59 eV for N_s^{-} and 0.75 eV for N_i^{-} (ΔE_d in Figure 4) to be compared to 0.14 eV for $N_s^{\bullet}$ and 0.73 eV for $N_i^{\bullet}$ (ΔE_p in Figure 4). The $N_s^{\bullet}-N_s^{-}$ shift of about 0.4 eV for substitutional nitrogen is caused by the fact that, in this case, the orbital where the extra electron is accommodated is a localized atomic-like orbital; instead the shift is almost negligible for interstitial nitrogen because the added electron occupies a more extended π molecular orbital. On the basis of these data, no significant variations in the absorption spectrum of the doped material are expected as a consequence of the internal charge transfer from the oxygen vacancies derived states to the N-impurity states, in particular if the species present are interstitial N atoms, $N_i^{\bullet}$ or N_i^{-}.

Another important aspect of the interaction between N-centers and oxygen vacancies (V$_O$) is that the energetically favorable charge transfer from Ti^{3+} ions to $N_b^{\bullet}$ centers is likely the reason why the cost of V$_O$ formation in bulk TiO$_2$ is largely reduced in the presence of N-impurities.[23] Indeed, the computed energy

(39) Hagfeldt, A.; Grätzel, M. *Chem. Rev.* **1995**, *95*, 49−68.
(40) Hoffmann, M. R.; Martin, S. T.; Choi, W.; Bahnemann, D. W. *Chem. Rev.* **1995**, *95*, 69−96.
(41) Linsebigler, A. L.; Lu, G.; Yates, J. T., Jr. *Chem. Rev.* **1995**, *95*, 735−758.

(42) See, A. K.; Bartynsky, R. A. *J. Vac. Sci. Technol., A* **1992**, *10*, 2591−2596.
(43) Henderson, M. A.; Epling, W. S.; Peden, C. H. F.; Perkins, C. L. *J. Phys. Chem. B* **2003**, *107*, 534−545.
(44) Serwicka, E.; Schlierkamp, M. W.; Schindler, R. N. *Z. Naturforsch.* **1981**, *36a*, 226−232.
(45) Berger, T.; Sterrer, M.; Diwald, O.; Knözinger, E.; Panayotov, D.; Thompson, T. L.; Yates, J. T., Jr. *J. Phys. Chem. B* **2005**, *109*, 6061−6068.
(46) Hurum, D. C.; Agrios, A. G.; Gray, K. A.; Rajh, T.; Thurnauer, M. C. *J. Phys. Chem. B* **2003**, *107*, 4545−4549.
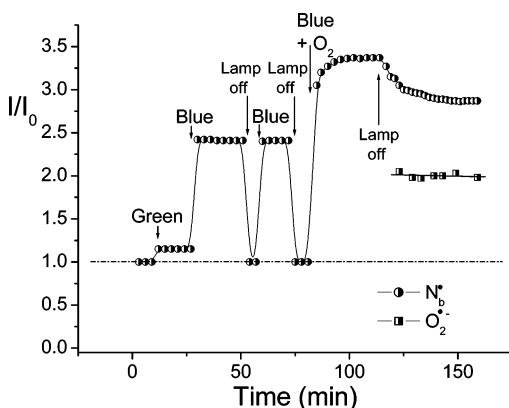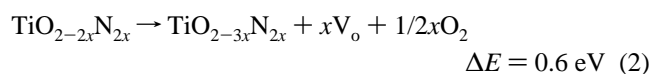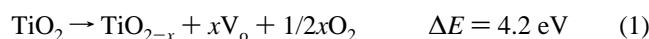
Figure 5. EPR signal intensity of $N_b^\bullet$ and $O_2^{\bullet-}$ in various conditions. $I_0 = 1$ is the $N_b^\bullet$ intensity in the non-irradiated sample.

cost to create oxygen vacancies is drastically reduced from 4.2 eV in pure TiO_2 to 0.6 eV in N-doped TiO_2, as indicated by the computed energetics for the following processes:[23]

$$TiO_2 \rightarrow TiO_{2-x} + xV_o + 1/2xO_2 \qquad \Delta E = 4.2 \text{ eV} \qquad (1)$$

$$TiO_{2-2x}N_{2x} \rightarrow TiO_{2-3x}N_{2x} + xV_o + 1/2xO_2$$
$$\Delta E = 0.6 \text{ eV} \quad (2)$$

Thus, DFT calculations suggest that N-doping favors O vacancy formation. Such a finding has been very recently confirmed by real-time transmission electron microscopy (TEM) experiments.[47] A consequence of the relatively higher number of oxygen vacancies in N-TiO_2, especially in oxygen-poor conditions,[48] is the partial quenching of the paramagnetic N-impurities ($N_b^\bullet$) which are transformed in $N_b^\bullet$. This is in agreement with the previously mentioned experimental observation that the EPR features related to $N_b^\bullet$ centers disappear upon reduction of the sample by annealing *in vacuo*, and reappear upon reoxidation. Similarly, recent experiments have found that N-implantation reduces the features associated to Ti^{3+} ions.[17] All these results suggest that N-TiO_2 contains, besides a given number of paramagnetic $N_b^\bullet$ centers, a fraction of diamagnetic $N_b^\bullet$ impurities, which depends on the level of oxygen deficiency in the sample.

3.4. EPR Spectra under Irradiation. To further clarify the role of diamagnetic and paramagnetic $N_b^\bullet$ species in the photoactivity of N-doped TiO_2, we have studied their behavior under irradiation *in vacuo* and in oxygen atmosphere, using light in the visible range. In particular, we have used two different wavelengths, one in the blue, $\lambda = 437$ nm, and the other, $\lambda = 500$ nm, in the green region of the visible spectrum (see Figure 1). The first wavelength roughly corresponds to the maximum absorption of the system, while the second one corresponds to the tail of the absorption band. Figure 5 reports the intensity of the observed EPR signals. The intensity scale is in arbitrary units, with the intensity of $N_b^\bullet$ in N-TiO_2 before irradiation normalized to 1.

From inspection of Figure 5 the following facts emerge:

(a) The EPR signal of $N_b^\bullet$ is not (or poorly) affected by irradiation with green light which causes just a small increase of the signal intensity. Using blue light of similar intensity the

EPR signal of $N_b^\bullet$ grows by a factor of about 2.3. This higher intensity remains constant until the lamp is turned off, when the signal recovers the initial value. The described behavior is thus completely reversible, and the signal grows again as the lamp is turned on.

(b) When the irradiation at 437 nm is performed in oxygen atmosphere ($p(O_2) = 5$ kPa), the increase of the $N_b^\bullet$ signal is accompanied by the simultaneous appearance of new EPR lines in the same spectral region (Figure 3b), which are due to two very similar surface superoxide $O_2^{\bullet-}$ radical species (Table 1). In particular the negative oxygen species are stabilized on two distinct surface Ti^{4+} ions (as indicated by their g_{zz} components at 2.025 and 2.023 respectively) which slightly differ one from the other in terms of coordinative environment (see Table 1). The observed g values are the same reported in the case of $O_2^{\bullet-}$ on TiO_2 generated by oxygen adsorption on the thermally reduced solid.[49] The experimental spectrum in Figure 3b and those successively recorded in the experiment (Figure 5, right-hand side) were deconvoluted in the three signals (Figure 3; c, c′, c″) by computer simulation. The quantitative evaluation of $O_2^{\bullet-}$ (species c and c′) was performed only after turning off the irradiation since, in such conditions, it is possible to evacuate O_2 from the gas phase without altering the relative abundance of the various species. In fact the presence of gas-phase O_2 reduces the accuracy of the quantitative measure of a surface paramagnetic species. This method allows us to evaluate the weight of all components ($N_b^\bullet$ and $O_2^{\bullet-}$) contributing to the "mixed" signal and, therefore, to derive the intensity data reported in the right-hand side of Figure 5. The formation of superoxide is irreversible at room temperature. Upon turning the lamp off the intensity value of $N_b^\bullet$ remains higher than the initial value recorded in the dark prior to oxygen adsorption. For the sake of comparison, we have also investigated the behavior under irradiation of the undoped TiO_2, prepared via sol−gel (see Experimental Section). As expected for this sample, adsorbed $O_2^{\bullet-}$ ions are abundantly formed under UV irradiation. However, under visible light irradiation of 437 nm, only a tiny superoxide signal is observed which is about 1 order of magnitude weaker (see Supporting Information) than the corresponding feature for the N-TiO_2 sample reported in Figure 3b. Therefore, we conclude that the formation of superoxide ions under irradiation at 437 nm in the presence of O_2 is typical of N-doped TiO_2 materials.

3.5. Visible Light-Induced Photoactivity in N-TiO_2: A Mechanistic View. The experimental and theoretical results presented in this paper allow us to draw a schematic picture of the mechanism connected to the interaction of N-TiO_2 with visible light.

(a) EPR investigations of N-TiO_2 reveal the presence of paramagnetic centers consisting of single N atoms localized at interstitial and/or substitutional positions of the bulk oxide lattice. Independent of its specific character, the $N_b^\bullet$ center introduces localized electronic states in the gap which can be either doubly occupied (diamagnetic N_b^-) or singly occupied (paramagnetic $N_b^\bullet$). The existence of EPR silent diamagnetic N_b^- centers is strongly supported by theoretical calculations (section 3.3) showing that there is a large energy gain associated to the transfer of an electron from a Ti^{3+} state to a singly occupied $N_b^\bullet$. The same conclusion is experimentally supported

(47) Sutter, E.; Sutter, P.; Fujita, E.; Muckerman, J. *Abstracts of the European Materials Research Society Spring Meeting*, Nice, France, 2006. Page M-14.
(48) Di Valentin, C.; Pacchioni, G.; Selloni, A. *Chem. Mater.* **2005**, *17*, 6656−6665.

(49) Che, M.; Tench, A. J. *Adv. Catal.* **1983**, *32*, 1−147.

by at least two facts: (i) the reversible decrease of the intensity of the $N_b^\bullet$ EPR signal upon reduction of the solid (section 3.2) due to the following process

$$N_b^\bullet + Ti^{3+} \leftrightarrow N_b^- + Ti^{4+} \tag{3}$$
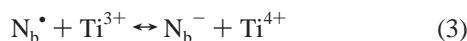
and (ii) the intensity increase of the same signal upon irradiation in vacuo or in O_2 which can be uniquely explained in terms of electron transfer from diamagnetic N_b^- centers (vide infra).
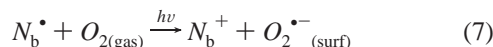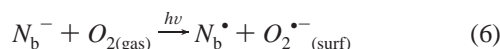
(b) Irradiation with visible light at 437 nm (2.84 eV) selectively promotes electrons from these states to the conduction band according to the following process:

$$N_b^- \xrightarrow{h\nu} N_b^\bullet + e^- \tag{4}$$

$$N_b^\bullet \xrightarrow{h\nu} N_b^+ + e^- \tag{5}$$

The fact that before irradiation EPR shows the presence of $N_b^\bullet$ centers in the sample is not in contradiction with the theoretical prediction of a higher stability of the N_b^- centers. This indeed suggests that the number of N impurities exceeds that of oxygen vacancies and that not all N paramagnetic centers are quenched by the charge-transfer mechanism.

The energy of the visible light is not sufficient to excite electrons from the valence band, as the TiO_2 anatase band gap is 3.2 eV. However, as reported above (section 3.3), DFT calculations show that the N-induced defect states lie a few tenths of an eV above the valence band edge in the case of both paramagnetic and diamagnetic charged species. Diamagnetic N_b^- species are expected to be definitely more abundant because they are energetically favored and are thus preferentially excited (reaction 4) so that under irradiation the equilibrium attained involves an increase of the concentration of the $N_b^\bullet$ paramagnetic centers (Figure 5). The equilibrium conditions in the dark are recovered instantaneously when irradiation is stopped.

(c) The presence of oxygen in the gas phase modifies the situation as a fraction of photoexcited electrons is scavenged by O_2, producing adsorbed $O_2^{\bullet-}$:

$$N_b^- + O_{2(gas)} \xrightarrow{h\nu} N_b^\bullet + O_2^{\bullet-}{}_{(surf)} \tag{6}$$

$$N_b^\bullet + O_{2(gas)} \xrightarrow{h\nu} N_b^+ + O_2^{\bullet-}{}_{(surf)} \tag{7}$$

This shifts the equilibrium with formation of a higher amount of paramagnetic $N_b^\bullet$ centers with respect to simple irradiation in vacuo. At this stage of the experiment the number of paramagnetic states observed in the system reaches its maximum value as the increase of $N_b^\bullet$ is accompanied by $O_2^{\bullet-}$ formation. In other words, photoinduced charge separation has occurred. The generation of surface adsorbed $O_2^{\bullet-}$ causes the formation of a negative layer at the interface. This, in turn, is expected to cause band bending which limits further electron transfer. Stopping irradiation, the electrons scavenged by oxygen remain in the ad-layer so that the initial concentration of $N_b^\bullet$ centers is not recovered. *The difference between the final and the initial amounts of $N_b^\bullet$ is rather close to the observed amount of generated $O_2^{\bullet-}$.* This reinforces the idea that most of the surface scavenged electrons are excited from N_b^- states.

4. Conclusions

The reported experiments show that $N_b^\bullet$ centers (single atom nitrogen centers in the bulk of titanium dioxide) play an essential
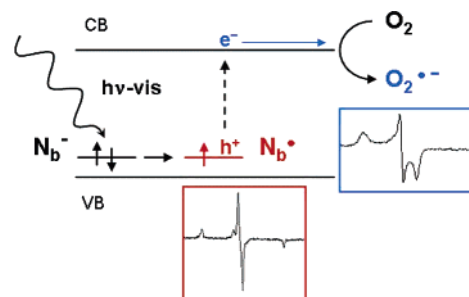

Figure 6. Sketch of the proposed mechanism for the processes induced by vis-light irradiation of the N-doped sample in O_2 atmosphere.

role in the absorption of visible light, in the promotion of electrons to the conduction band, and in photoinduced electron transfer to reducible adsorbates. Both neutral paramagnetic $N_b^\bullet$ and charged diamagnetic N_b^- are present and introduce localized N-states a few tenths of an eV above the valence band. $N_b^\bullet$ paramagnetic centers in the presence of oxygen vacancies form N_b^- diamagnetic precursors at the expenses of the Ti^{3+} ions which are oxidized to Ti^{4+}. DFT calculations show that this is an effective process as the formation energy of oxygen vacancies is drastically reduced by N-doping. Visible light of 437 nm causes excitation of electrons mainly from the diamagnetic N-centers. These electrons reversibly occupy delocalized conduction band states (when the irradiation is performed in vacuo) or are irreversibly transferred onto an adsorbed electron scavenger like oxygen (irradiation in a O_2 atmosphere). This mechanistic picture is sketched in Figure 6. It is therefore demonstrated that among the various species which form during the synthesis of N-TiO₂, the bulk N_b centers in the anatase matrix are photoactive centers, and likely the only ones capable of visible light absorption and molecular photoactivation.

The visible light-induced charge separation here described is analogous, in N-TiO₂, to the classical experiment induced by UV light in bare TiO₂. In the latter case, however, both the electron and the hole formed are delocalized and available for redox processes at the surface as shown in the classic experiment reported by Howe and Grätzel.[50] In the case of N-TiO₂, however, the hole formed by charge separation remains localized onto the center, which becomes a $N_b^\bullet$ (or N_b^+) center. Photoexcited electrons are available for chemical interactions at the surface. The same does not hold for the hole,[51,52] and this fact constitutes a potential limit of the activity of the N-TiO₂ system in photocatalytic processes which are usually based on the parallel reductive/oxidative action of the electron and hole respectively.

The picture here proposed holds for systems prepared by sol−gel reactions and, very likely, for other chemically prepared N-TiO₂ systems. It cannot be excluded however, that for systems prepared by radically different techniques other types of centers are formed, and other mechanisms of photoactivation apply.

Supporting Information Available: The superoxide formation at the surface under irradiation; the comparison between undoped and N-doped TiO₂. This material is available free of charge via the Internet at http://pubs.acs.org

JA064164C

(50) Grätzel, M.; Howe R. F. *J. Phys. Chem.* **1990**, *94 (6)*, 2566−2572.
(51) Mrowetz, M.; Balcerski, W.; Colussi, A. J.; Hoffmann, R. *J. Phys. Chem. B* **2004**, *108*, 17269−17273.
(52) Nakamura, R.; Tanaka, T.; Nakato, Y. *J. Phys. Chem. B* **2004**, *108*, 10617−10620.